

Geometry-Aware Scene-Consistent Image Generation

Cong Xie* Che Wang* Yan Zhang Zheng Pan Han Zou Zhenpeng Zhan
Global Business Unit, Baidu Inc.

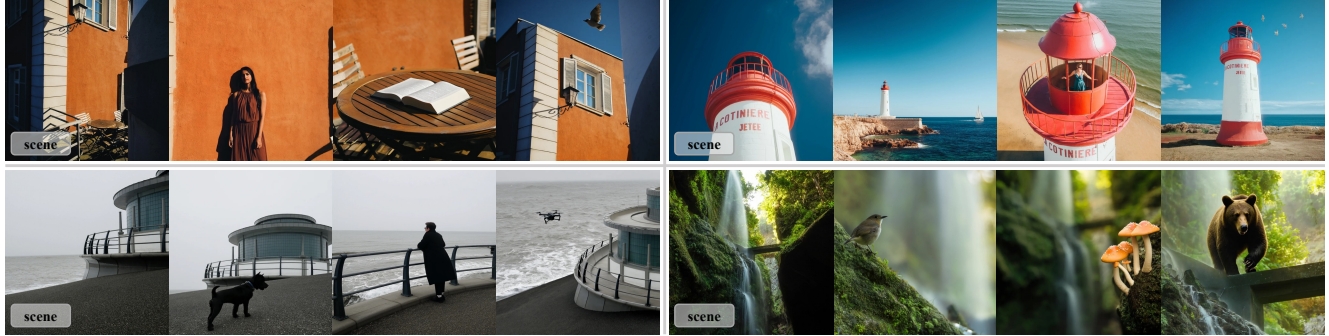


Figure 1. Geometry-aware scene-consistent image generation. Images labeled with the subscript “scene” are reference scene images used to guide generation; the remaining images are our results, which depict diverse viewpoints while remaining consistent with the underlying scene geometry, rather than merely copying the reference.

Abstract

We study geometry-aware scene-consistent image generation: given a reference scene image and a text condition specifying an entity to be generated in the scene and its spatial relation to the scene, the goal is to synthesize an output image that preserves the same physical environment as the reference scene while correctly generating the entity according to the spatial relation described in the text. Existing methods struggle to balance scene preservation with prompt adherence: they either replicate the scene with high fidelity but poor responsiveness to the prompt, or prioritize prompt compliance at the expense of scene consistency. To resolve this trade-off, we introduce two key contributions: (i) a scene-consistent data construction pipeline that generates diverse, geometrically-grounded training pairs, and (ii) a novel geometry-guided attention loss that leverages cross-view cues to regularize the model’s spatial reasoning. Experiments on our scene-consistent benchmark show that our approach achieves better scene alignment and text–image consistency than state-of-the-art baselines, according to both automatic metrics and human preference studies. Our method produces geometrically coherent images with diverse compositions that remain faithful to the textual instructions and the underlying scene structure.

1. Introduction

Generating diverse yet scene-consistent images, where the underlying physical environment remains coherent across changes in viewpoint or composition, is a critical challenge in generative AI. Such scene-consistent image generation is a critical research problem in computer vision generation, with broad applications in comic generation [19, 24–26, 42, 49] where consistent backgrounds ensure narrative coherence; temporal video editing [9, 11, 15, 32, 44], such as synthesizing start and end frames for image-to-video generation; and immersive Augmented Reality / Virtual Reality (AR/VR) [14, 30] environments, where novel-view generation demands consistent scene structure to preserve immersion and spatial awareness.

Despite significant progress in generative image generation, geometry-aware scene consistency remains a major challenge. While local image inpainting [13, 18, 40, 41] can perform localized edits and maintain consistency to some extent, it mainly targets filling missing regions or adding local content. For example, in comic generation, advancing the storyline often requires changing the scene’s perspective and composition. Local inpainting, however, cannot reliably transform a scene from a frontal view to an oblique view while preserving the geometric consistency of the background. Furthermore, 3D reconstruction [7, 12, 17] methods preserve multi-view consistency but rely on accurate camera parameters, involve high interaction costs, and

*Equal contribution.

are limited in generating images according to given textual descriptions.

Existing text-driven image editing models [10, 21, 29, 38] are typically designed as general-purpose, multi-task frameworks, enabling diverse semantic modifications yet lacking explicit optimization for scene consistency. Moreover, they struggle to balance scene preservation with prompt adherence, either replicating the scene with high consistency but poor responsiveness to the prompt, or prioritizing prompt compliance at the expense of scene consistency. Such limitations largely result from the lack of fine-tuning on datasets incorporating scene consistency constraints and from employing generic training objectives rather than ones specialized for the task.

Constructing scene-consistent training data is non-trivial. To be effective, training pairs must satisfy two key properties: (i) the ground-truth entities to be generated in the scene must exhibit physically plausible spatial and scale relationships with the underlying environment, and (ii) the input and output views, while depicting the same underlying physical environment, may differ in viewpoint or layout as dictated by the text condition (e.g., the text may request a top-down view of the scene even when the reference image is a low-angle view, as in the lighthouse example in Figure 1). An intuitive strategy is to start from real-world multi-view datasets with scene annotations and camera poses, such as DL3DV-10K [22], and then composite people or objects into each view. However, because the entities are not captured in the original imagery, naive compositing often leads to scale mismatch, lighting inconsistency, and blending artifacts at object boundaries, which breaks the physically correct entity–scene relationships and degrades supervision quality. Another option is to mine frame pairs from web videos, but shot changes and scene transitions frequently mean that two frames do not depict the same physical scene at all; restricting to adjacent frames preserves scene identity but collapses the viewpoint baseline, yielding pairs with almost identical geometry and thus failing to teach the model how to maintain consistency under meaningful camera or layout changes. Moreover, for long shots, even frames within the same shot can drift across locations or compositions, making it difficult to control whether sampled pairs truly correspond to a single, consistent physical scene.

To overcome these limitations, we introduce a scene-consistent data construction pipeline that directly uses real photographs as training targets and leverages video generation models to synthesize geometrically diverse yet scene-consistent views. Concretely, we treat real-world images containing people or objects as target views, ensuring that entity–scene spatial relationships, scales, and contacts are physically correct by construction. We then employ a video generation model to produce short clips that evolve the cam-

era and composition around the same scene. This yields paired reference–target views that jointly satisfy both requirements: realistic entity–scene spatial relationships and cross-view geometric variation. Building on these data, we further propose a geometry-guided attention loss that exploits estimated cross-view correspondence cues between the reference scene and the target view to regularize intermediate attention maps. By encouraging attention to focus on geometrically corresponding regions across views, this loss explicitly guides the model to preserve scene structure and appearance as the viewpoint and composition change.

Our contributions are summarized as follows:

1. We propose a stable scene dataset construction method that generates high-quality, scene-consistent paired data with precise text–image alignment. This pipeline overcomes key obstacles in constructing training pairs that simultaneously preserve a shared underlying scene geometry, maintain physically plausible entity–scene relationships, and support substantial viewpoint and layout variation.
2. We introduce a geometry-guided attention loss that leverages cross-view correspondence cues to regularize attention and strengthen scene consistency.
3. We demonstrate that our method achieves superior performance to existing approaches across multiple scene-consistency metrics and qualitative evaluations.

2. Related Works

Consistency generation based on diffusion models has experienced rapid development. Existing studies related to scene-consistent image generation can be broadly categorized into three main directions: reference-based feature adaptation, text-driven image editing, and 3D reconstruction with viewpoint control.

Reference-Based Feature Adaptation Methods These methods encode features from a reference image and fuse them with text features via cross-attention to enforce appearance/structure consistency. Recent approaches such as IP-Adapter [45], Fastcomposer [39], MagicTailor [48], PhotoMaker [20], InstantID [34], Stydeco [43] and StyleAdapter [35] incorporate multi-reference fusion and identity/style conditioning to improve stability and cross-image consistency in image generation. Other techniques, including local patch matching (e.g. Paint-by-Example [41], Blended Latent Diffusion [1]), and conditional guidance networks like ControlNet [46], offer finer control over reference conditioning. However, these methods generally focus on transferring specific attributes from the reference image and lack the capability to handle viewpoint changes or maintain geometry-aware scene consistency.

Text-Driven Image Editing Methods Approaches such as FLUX.1 Kontext Dev [16], Qwen-Image-Edit [37], See-dream [29], Uniworld-V2 [21], DreamOmni2 [38], Instruct-pix2pix [2], and Dual-Schedule Inversion [10] are typically trained on large-scale image–text datasets encompassing a wide range of editing operations. These datasets include diverse tasks such as object insertion and removal, style transfer, background replacement, and spatial layout adjustment, enabling the models to learn generalizable editing capabilities. Leveraging text prompts as the primary control signal, these methods can perform both local and global modifications. While such broad coverage grants strong versatility, it also introduces a fundamental limitation for tasks requiring strict scene fidelity. The mixed-task nature of the training data encourages the model to apply global changes to the entire image in response to textual instructions, rather than isolating edits to specific target regions such as scene layout.

3D Reconstruction Methods These methods leverage explicit geometric cues and camera parameter conditioning to enforce multi-view consistency, integrating camera intrinsics and view control with reconstruction to generate consistent images across viewpoints. Generative Photography [12] and CameraCtrl [7] require accurate camera parameters such as focal length, aperture, and field of view to guide generation, enabling geometrically consistent outputs in professional photography or virtual production. ControlNeRF [17] employs neural radiance fields (NeRF) for scene modeling and renders multiple views from specified poses, while VistaDream [33] reconstructs a 3D scene from a single image and synthesizes novel viewpoints to preserve scene consistency. Although excellent in viewpoint controllability and geometric fidelity, these methods generally incur high interaction costs, depend on expert-level parameter input, and focus primarily on viewpoint transitions or scene restoration. They lack the capability to generate images according to given textual descriptions, such as introducing new characters or enabling human–scene interactions, which constrains their applicability in flexible scene-consistent generation scenarios.

In summary, existing methods advance multiple aspects but lack simultaneous capability of generating images according to given textual descriptions and geometry-aware scene preservation. This gap motivates our proposed framework, which combines high-quality scene-consistent data construction with explicit attention-based modeling. Notably, SceneDecorator [31] is **the most relevant work** to our framework, which focuses on scene-oriented story generation, employing a training-free global-to-local scene planning strategy and long-term scene-sharing attention to maintain cross-story scene consistency. While SceneDecorator is designed for scene-oriented story generation, prior-

itizing global scene planning and narrative coherence, our framework addresses the distinct task of scene-consistent semantic editing, where fine-grained modifications must follow the textual description while maintaining geometry–scene consistency.

3. Methods

3.1. Overview

Given a reference scene image I_{scene} and a text condition c that specifies both the entity to be generated in the scene and its spatial relationship to the scene, our goal is to generate a scene-consistent output image I_{out} that (i) depicts the same physical scene as I_{scene} , and (ii) correctly generates the entity according to the spatial relation described in the text. We denote the generative model as

$$I_{\text{out}} = f_{\theta}(I_{\text{scene}}, c), \quad (1)$$

where f_{θ} is implemented as a diffusion-based image generator conditioned on both the reference scene and the text.

As illustrated in Figure 2, our method has two components. First, we build a scene-consistent data construction pipeline that converts real world images into multi-view tuples comprising entity-removed scenes, synthesized scene views, and soft geometric correspondence masks. Second, during training we apply a geometry-guided attention loss that uses these correspondence cues to regularize intermediate attention maps, encouraging attention to focus on geometrically corresponding regions across views and thereby better preserving scene structure.

3.2. Scene-Consistent Data Construction

Directly collecting large-scale triplets $(I_{\text{scene}}, c, I_{\text{out}})$ with explicit viewpoint changes and consistent scenes is challenging, since each triplet must satisfy both realistic entity–scene geometry and cross-view geometric variation. Instead, we derive supervision from real-world photographs combined with an off-the-shelf video diffusion model [32] trained on large-scale videos with natural camera motion, which provides realistic cross-view variation and soft geometric correspondences while approximately preserving scene identity.

Entity Removal from Single Images We start from large photo collections containing humans and generic objects in diverse scenes. For each image I_{full} , we automatically erase a target entity region (person or object) to obtain an entity-removed scene \tilde{I}_{scene} . For human-centric photos, we apply FLUX.1 Kontext Dev [16] for person removal, and additionally apply face detection [6] and human segmentation [23, 27] to discard low-quality results and maintain high-quality entity-removed scenes. For non-human

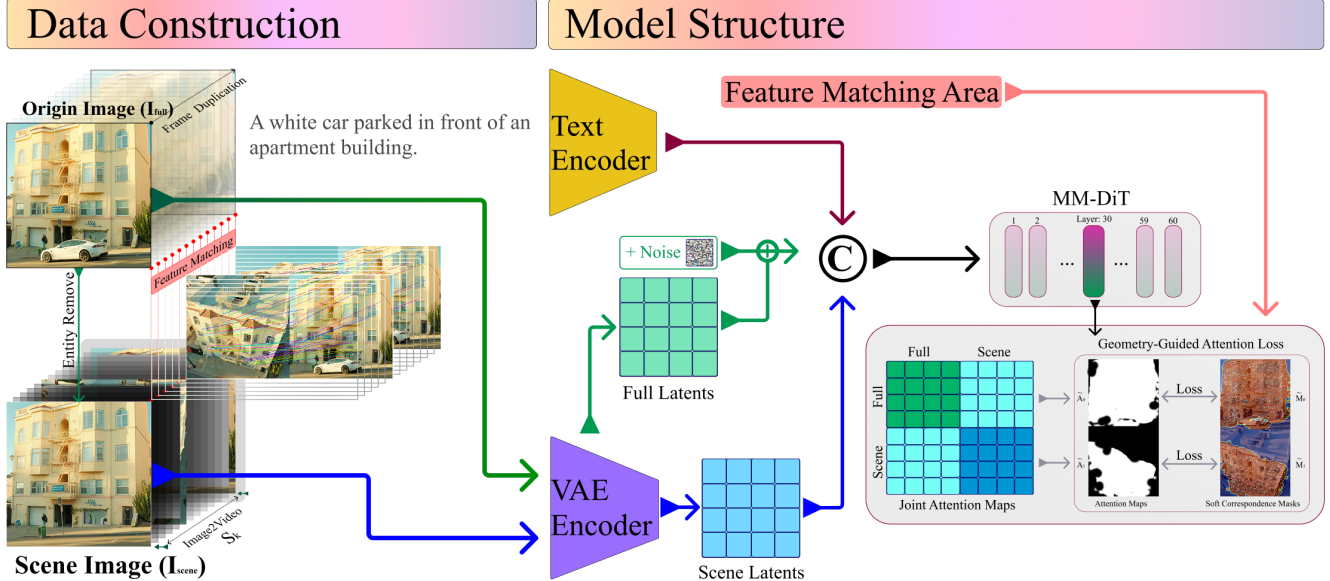


Figure 2. Overall framework of our method with two contributions: (a) Scene-Consistent Data Construction Pipeline, generating high-quality, scene-consistent paired data with precise text–image alignment; (b) Geometry-Guided Attention Loss, encouraging attention to focus on geometrically corresponding regions to better preserve scene structure.

objects, we use open-source image-editing datasets OmniEdit [36] that provide object-removal image pairs. The resulting \tilde{I}_{scene} images serve as realistic scene-only inputs for the subsequent multi-view synthesis stage.

Multi-View Scene Generation via Image-to-Video
Given \tilde{I}_{scene} , we employ a pre-trained image-to-video diffusion model \mathcal{G}_{i2v} (Wan 2.2 [32]) to synthesize a short video sequence

$$\{S_k\}_{k=0}^{K-1} = \mathcal{G}_{\text{i2v}}(\tilde{I}_{\text{scene}}), \quad (2)$$

where each frame S_k corresponds to the same underlying scene under a slightly different camera motion.

Benefiting from large-scale training on real-world videos, the image-to-video diffusion model \mathcal{G}_{i2v} can transform a single high-quality photograph into a short clip with physically plausible and coherent camera motion. In our pipeline, this allows any still image to be converted into a compact multi-view sequence, greatly expanding the pool of training scenes and naturally enriching scene viewpoints.

For each source image I_{full} , we pair it with one of the synthesized frames S_k to form a scene pair (I_{full}, S_k) . In our training formulation, S_k plays the role of I_{scene} , while I_{full} serves as a proxy for I_{out} .

Geometry Extraction with Feature Matching To obtain explicit scene-level correspondence cues between I_{full} and the selected scene view S_k , we apply a pre-trained feature matching network [28] that estimates sparse correspondences between two views of the same scene under viewpoint changes. Given the pair (I_{full}, S_k) , the matcher outputs

$$\{(x_i^0, y_i^0)\}_{i=1}^N, \quad \{(x_i^1, y_i^1)\}_{i=1}^N, \quad (3)$$

where (x_i^0, y_i^0) and (x_i^1, y_i^1) denote coordinates of matched points in I_{full} and S_k , respectively.

We convert these sparse matches into dense, soft correspondence masks. Let $H \times W$ be the image resolution and $K \in \mathbb{R}^{(2r+1) \times (2r+1)}$ be a radial kernel (e.g., Gaussian) whose values decay with distance from the center. For each match $((x_i^0, y_i^0), (x_i^1, y_i^1))$, we add a copy of K centered at (x_i^0, y_i^0) and (x_i^1, y_i^1) onto masks $M_0, M_1 \in \mathbb{R}^{H \times W}$, respectively, accumulating overlapping contributions and clipping them to a fixed range. We then crop and downsample M_0 and M_1 to the spatial resolution of the latent feature maps used for attention supervision, obtaining

$$\tilde{M}_0, \tilde{M}_1 \in \mathbb{R}^{H_s \times W_s}. \quad (4)$$

High responses in \tilde{M}_0 and \tilde{M}_1 highlight regions that are geometrically corresponding between the two views.

3.3. Geometry-Guided Attention Loss

We build on the state-of-the-art image editing model Qwen-Image-Edit [37] and augment it with geometry-guided attention supervision.

MMDiT Backbone Our model adopts the double-stream Multimodal Diffusion Transformer (MMDiT) architecture

of Qwen-Image-Edit, jointly modeling noise and image latents under text conditioning. Given a noisy latent of the target image I_{full} (proxy for I_{out}), a reference scene image I_{scene} , and a text prompt c describing the inserted entity, the model predicts the added noise by using two streams: one for image tokens, and another for conditioning tokens (which jointly encode the scene and the text).

We keep the variational autoencoder (VAE), text encoder, and backbone weights of Qwen Image Edit frozen, and only introduce a small number of trainable parameters via lightweight adapters. This parameter-efficient fine-tuning preserves the strong priors of the base model while enabling specialization to our scene-consistent editing objective and the proposed geometry-aware attention regularization.

Geometry-Guided Attention Loss Given the source image I_{full} (denoted as view 0) and the scene condition S_k (denoted as view 1), we extract their visual tokens from an intermediate attention layer of MMDiT, $z_0 \in \mathbb{R}^{L_0 \times d}$, $z_1 \in \mathbb{R}^{L_1 \times d}$, where L_0 and L_1 denote the number of tokens for view 0 and view 1, respectively, and d is the token feature dimension. We then form a joint token sequence $X = [z_0; z_1] \in \mathbb{R}^{(L_0+L_1) \times d}$, and use it as both queries and keys, $Q = K = X$. The attention score matrix is computed as

$$A = \text{softmax}\left(\frac{QK^\top}{\sqrt{d}}\right) \in \mathbb{R}^{(L_0+L_1) \times (L_0+L_1)}.$$

We denote by $\mathcal{I}_0 = \{1, \dots, L_0\}$ the index set of tokens from view 0 and by $\mathcal{I}_1 = \{L_0 + 1, \dots, L_0 + L_1\}$ the index set of tokens from view 1. Each entry A_{ij} represents the attention weight assigned by token i to token j . In particular, for $i \in \mathcal{I}_0$ and $j \in \mathcal{I}_1$, A_{ij} encodes the attention from a token in view 0 to a token in view 1, while A_{ji} with $j \in \mathcal{I}_1$ and $i \in \mathcal{I}_0$ encodes the reverse direction. In our setting, we expect tokens that correspond to the same scene location across views to allocate higher attention to each other, so that geometrically matching regions are emphasized in the cross-view attention map. If a token $p \in \mathcal{I}_0$ participates in a successful keypoint correspondence, its counterpart in \mathcal{I}_1 will exhibit a similar visual feature. As a result, both the attention that p allocates to tokens $q \in \mathcal{I}_1$ and the attention it receives from them tend to be higher. We therefore summarize its cross-view interaction by symmetrizing and averaging these two directions as

$$a_p^{(0)} = \frac{1}{2} \left(\frac{1}{L_1} \sum_{q \in \mathcal{I}_1} A_{pq} + \frac{1}{L_1} \sum_{q \in \mathcal{I}_1} A_{qp} \right), \quad q \in \mathcal{I}_1.$$

Since the keypoint-based correspondence map \tilde{M}_0 assigns a high value to the location of token p , we use it as

supervision in our loss, encouraging $a_p^{(0)}$ to take a similarly high value

$$\mathcal{L}_{\text{attn}0} = \frac{1}{N} \left(\left\| \tilde{A}_0 - \tilde{M}_0 \right\|_2^2 \right), \quad (\tilde{A}_0)_p = a_p^{(0)}. \quad (5)$$

Similarly, we apply the same supervision in the reverse direction from q to p , leading to the following attention loss:

$$\mathcal{L}_{\text{attn}1} = \frac{1}{N} \left(\left\| \tilde{A}_1 - \tilde{M}_1 \right\|_2^2 \right). \quad (6)$$

The geometry-guided attention loss is defined as

$$\mathcal{L}_{\text{attn}} = \mathcal{L}_{\text{attn}0} + \mathcal{L}_{\text{attn}1}, \quad (7)$$

where $N = H_s W_s$ denotes the number of spatial locations per view. This loss encourages the joint attention to place high mass on geometrically corresponding scene regions in both views, guiding the model to preserve underlying scene structure while editing according to the text and to produce viewpoint-consistent content. In practice, we apply this supervision only to a single mid-level joint-attention block, which empirically balances strong geometric guidance with sufficient flexibility in the remaining layers.

3.4. Training Objective

We train the model using a combination of the standard diffusion loss and the geometry-guided attention loss. Following common practice in latent diffusion, we add Gaussian noise with variance schedule σ_t^2 to the latent representation of the target image I_{full} at a randomly sampled timestep t , and train the network to predict the noise (or a reparameterization thereof) given the noisy latent, the reference scene S_k , and the text c .

Let ϵ denote the ground-truth noise and $\hat{\epsilon}_\theta$ the model prediction. The diffusion loss is

$$\mathcal{L}_{\text{diff}} = \mathbb{E}_{t, \epsilon} \left[w(t) \left\| \hat{\epsilon}_\theta - \epsilon \right\|_2^2 \right], \quad (8)$$

where $w(t)$ is a time-dependent weighting function determined by the variance schedule.

The total training objective is

$$\mathcal{L} = \mathcal{L}_{\text{diff}} + \lambda \mathcal{L}_{\text{attn}}, \quad (9)$$

where λ controls the strength of the geometry-guided attention supervision. In our experiments, we use a fixed λ (e.g., $\lambda = 3.0$), and apply $\mathcal{L}_{\text{attn}}$ only to selected attention blocks.

4. Experiments

4.1. Implementation Details

We construct our training set from Places365 [47] and OmniEdit [36], resulting in 96,040 distinct entity-centric scene

Table 1. Quantitative comparison of automatic metrics and user study across baselines. The best result is highlighted in **bold**.

Methods	Automatic Metrics		User Study	
	G2.5F-SA↑	G2.5F-TIA↑	Scene Align↑	Text Align↑
Qwen-Image-Edit [37]	9.434	9.306	34.89%	28.43%
FLUX.1 Kontext Dev [16]	8.395	8.841	26.29%	25.46%
SceneDecorator [31]	4.104	8.176	1.69%	17.67%
Ours	9.811	9.639	37.13%	28.45%

images. For each image, we generate a short video clip using Wan 2.2 [32], and apply the keypoint-based feature matcher MINIMA [28] to filter frames, retaining pairs that exhibit sufficient viewpoint change while preserving scene identity. On average, each source image contributes about 14 frames, yielding 1,336,509 scene pairs in total. Text descriptions for all samples are annotated using the GLM-4.1V-Thinking vision–language model [8].

We train the model on 8 NVIDIA H100 GPUs with a batch size of 1 per GPU and gradient accumulation over 6 steps, corresponding to an effective batch size of 48. We adopt multi-resolution training with arbitrary aspect ratios, constraining the longer image side to at most 1024 pixels (maximum resolution 1024×1024). The model is optimized for 4,000 steps. At inference time, we use 28 denoising steps.

We conduct a comparative evaluation of our method with three representative baselines: Qwen-Image-Edit [37], FLUX.1 Kontext Dev [16], and SceneDecorator [31]. The test set comprises 425 images collected from a variety of scene types. For each image, five distinct textual prompts are created using Gemini-2.5-Pro [3], yielding a total of 2,125 scene-prompt pairs. All competing methods run on this identical set of inputs to ensure comparability under consistent conditions.

4.2. Quantitative Comparisons

We quantitatively evaluate the effectiveness of our method through two complementary perspectives: objective assessment via automatic metrics and subjective evaluation via user studies.

Automatic Metrics We assess the quality of the generated image using Gemini 2.5 Flash [3], focusing on two aspects: (i) Gemini 2.5 Flash scene alignment (G2.5F-SA), which measures the scene consistency between the reference image and the generated frame, evaluating how well the generated content preserves the original physical environment without introducing undesired changes. Since our task involves text-guided image editing, edits such as object modifications, depth-of-field effects, zoom or rotation, and moderate viewpoint changes are considered acceptable and

are excluded from negative judgment when evaluating scene consistency, with the score focusing solely on the consistency of the scene background. (ii) Gemini 2.5 Flash text-image alignment(G2.5F-TIA), evaluates how faithfully the visuals follow the given textual prompt. Both metrics are scored on a scale from 0 (poor) to 10 (excellent). The detailed results are reported in Table 1 Our method achieves the highest scores among all compared approaches in both G2.5F-SA and G2.5F-TIA. These results demonstrate that our approach delivers the best overall performance in preserving scene integrity while accurately following the textual prompts. Previous work mainly relies on CLIP-T [5] and DreamSim [4] for evaluation, but we find that these metrics do not accurately capture our task; a detailed analysis is provided in the supplementary material.

User Study We carried out a user study on the 2,125 scene–prompt pairs using the corresponding outputs from all compared methods. The evaluation was conducted on an in-house crowdsourcing platform with 50 participants, yielding a total of 6,375 votes, where each scene–prompt pair was evaluated by three distinct annotators. For each scene–prompt pair, annotators were shown the reference scene and all candidate outputs, and were asked to assess each method according to two criteria: (i) text alignment and (ii) scene alignment. The scores reported in Table 1 are expressed as percentages, obtained by applying a temperature-scaled normalization to the aggregated votes. As shown in Table 1, our method achieves the highest preference under both text alignment and scene alignment. Compared to Qwen-Image-Edit [37], our approach is more frequently judged to produce images that both follow the textual instructions and preserve the underlying scene geometry and layout. We attribute these gains primarily to our scene-consistent data construction pipeline, which supplies training pairs with realistic entity–scene relationships and cross-view variations, thereby validating the effectiveness of our data design for improving scene consistency.

4.3. Qualitative Comparisons

Additionally, we conduct qualitative comparisons of our method with three existing approaches. The visualization

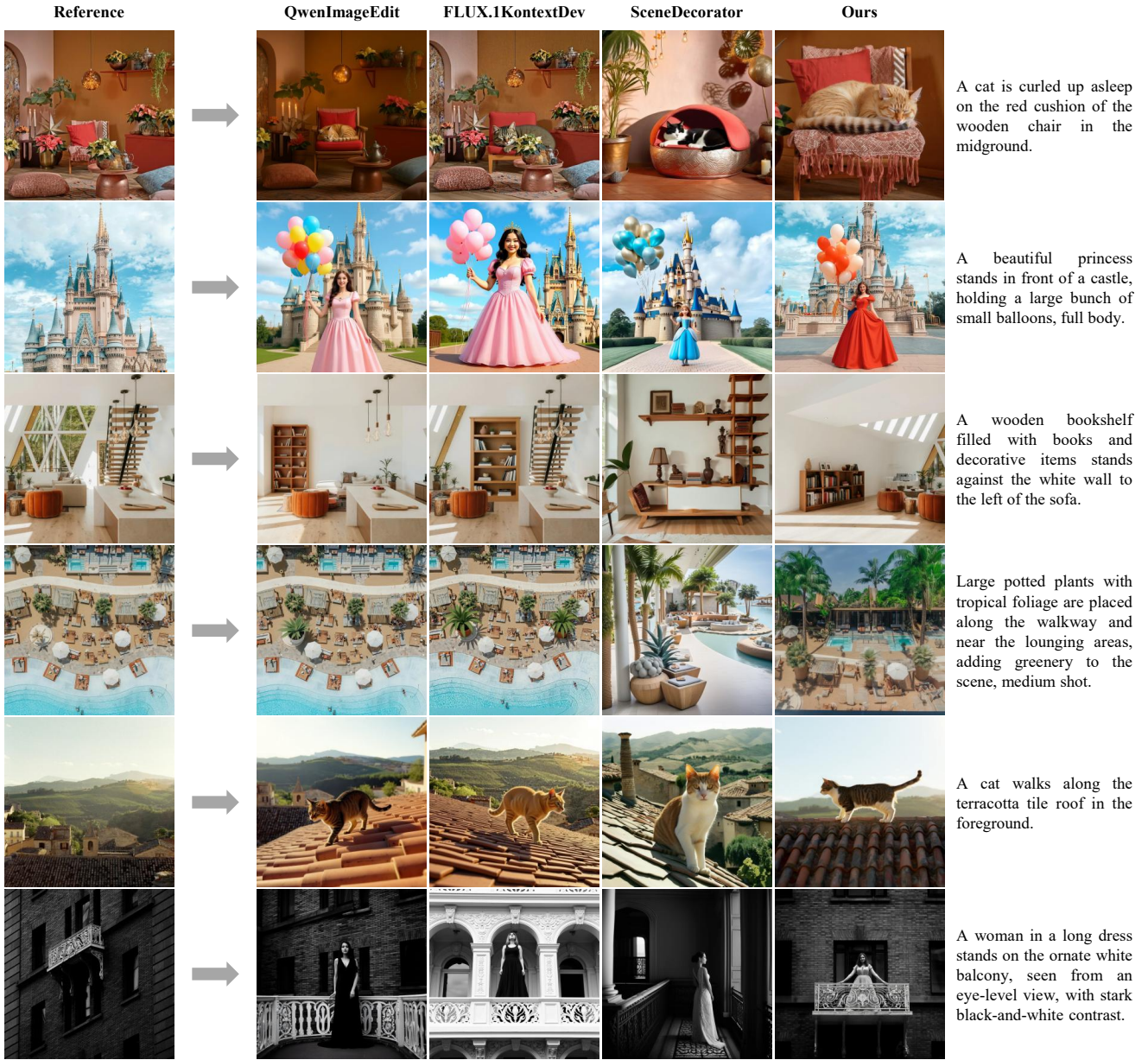


Figure 3. Qualitative comparison of our method with other baselines. Our method demonstrates superior scene consistency and text-image consistency compared to other baselines.

results are presented in Figure 3, with additional examples available in the supplementary material. While both Qwen-Image-Edit [37] and FLUX.1 Kontext Dev [16] respond to text-guided editing prompts, they often introduce subtle changes to surrounding regions, such as texture alterations, variations in color saturation, or modifications to small scene elements, and exhibit limited capability in spatial understanding. This is largely because these models are primarily designed for generic text-driven image editing without specialized training to preserve background consistency or handle spatial transformations of the background.

SceneDecorator [31], on the other hand, can maintain a roughly similar global scene layout, but its correspondence to the original scene is mostly at the element level. Many objects undergo noticeable changes in appearance, leading to reduced fidelity to the source scene. Our geometry-aware method captures fine-grained scene semantics while maintaining high scene consistency with the given prompt, demonstrating clear advantages in scene-consistent generation.

4.4. Analysis and Ablation Study

In this section, we evaluate the effectiveness of the two proposed components: geometry-guided attention loss and scene-consistent data construction pipeline.

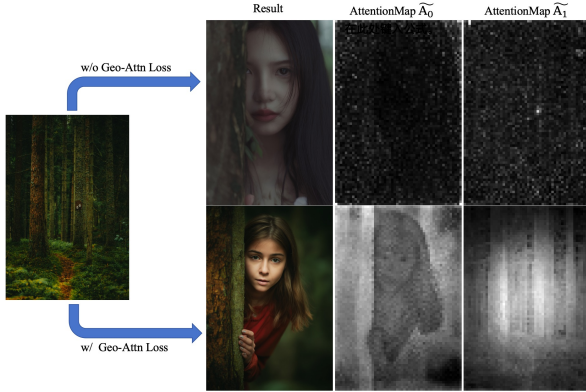


Figure 4. Generated image and attention map comparison with and without geometry-guided attention loss. (text prompt:a girl hiding behind a tree, close up)

Table 2. Ablation study of geometry-guided attention loss.

Methods	G2.5F-SA↑	G2.5F-TIA↑
w/o Geo-Attn Loss	9.532	8.569
w/ Geo-Attn Loss	9.811	9.639

Geometry-Guided Attention Loss Furthermore, the impact of the proposed geometry-guided attention loss can be observed in Table 2, which highlights its role in enhancing the coherence of generated scenes. With the attention loss, the model achieves improvements on both scene alignment and text–image alignment metrics, with G2.5F-SA increasing by 0.279 and G2.5F-TIA increasing by 1.07, which demonstrates its ability to maintain stable spatial relationships within the scene. In addition, we provide a visual comparison of generations with and without the proposed geometry-guided attention loss and analyze the attention maps from the designated mid-level block used to compute the loss, as shown in Figure 4. \tilde{A}_0 denotes the attention map between each pixel of the target scene and the input image, while \tilde{A}_1 denotes the attention map between each pixel of the scene image and the target image; brighter regions indicate higher correlation at the corresponding positions. With the attention loss, the attention maps highlight spatially corresponding regions in both images, indicating that the network has learned to focus on areas crucial for maintaining scene consistency. These observations collectively demonstrate that the attention loss not only improves visual scene

Table 3. Gemini 2.5 Flash evaluation of different data construction strategies.

Data	G2.5F-SA↑	G2.5F-TIA↑
DL3DV-10K [22]	9.048	8.960
ours	9.811	9.639

consistency but also guides the model to attend to geometrically relevant background regions.

Scene-Consistent Data Construction

We compare models trained with our Scene-Consistent Data Construction pipeline (Section 3.2) against a baseline built from real-world multi-view datasets with post-hoc entity insertion. For the baseline, we start from multi-view scene sequences in DL3DV-10K [22] and insert foreground humans or objects into the target views using FLUX.1 Kontext Dev [16], while keeping the network architecture, optimization hyperparameters, and training schedule identical. As reported in Table 3, training on our scene-consistent data yields consistently higher G2.5F-SA and G2.5F-TIA scores than the DL3DV-10K-based baseline, demonstrating the clear advantage of our scene-consistent data construction pipeline for cross-view editing. Although the DL3DV-10K-based baseline offers multi-view coverage of each scene, the composited images often exhibit instance-scale imbalance and related artifacts, which likely degrade supervision quality, as further discussed in the supplementary material.

5. Conclusion

This paper presents a geometry-aware framework for generating images that preserve the geometry of the reference scene, while generating entities aligned with the described spatial relation. Our contributions include: (i) a stable scene dataset construction method that produces high-quality, scene-consistent paired data with precise text–image alignment, enabling effective training with explicit scene consistency constraints; and (ii) a geometry-guided attention loss that leverages cross-view geometric correspondences to regularize intermediate attention maps, encouraging the model to focus on geometrically relevant regions, and thereby better preserving scene structure during generation. Extensive experiments across diverse scenarios demonstrate that our method achieves superior performance over existing approaches in both automatic metrics and user studies, with clear improvements in scene alignment and text–image consistency. Qualitative visualizations further confirm that our geometry-aware design effectively captures fine-grained scene semantics and maintains high scene consistency even under significant viewpoint changes.

References

[1] Omri Avrahami, Ohad Fried, and Dani Lischinski. Blended latent diffusion. *ACM transactions on graphics (TOG)*, 42(4):1–11, 2023. 2

[2] Tim Brooks, Aleksander Holynski, and Alexei A Efros. Instructpix2pix: Learning to follow image editing instructions. In *Proceedings of the IEEE/CVF conference on computer vision and pattern recognition*, pages 18392–18402, 2023. 3

[3] Gheorghe Comanici, Eric Bieber, Mike Schaeckermann, Ice Pasupat, Noveen Sachdeva, Inderjit Dhillon, Marcel Blissein, Ori Ram, Dan Zhang, Evan Rosen, et al. Gemini 2.5: Pushing the frontier with advanced reasoning, multimodality, long context, and next generation agentic capabilities. *arXiv preprint arXiv:2507.06261*, 2025. 6, 1, 2, 3

[4] Stephanie Fu, Netanel Tamir, Shobhita Sundaram, Lucy Chai, Richard Zhang, Tali Dekel, and Phillip Isola. Dreamsim: Learning new dimensions of human visual similarity using synthetic data. *arXiv preprint arXiv:2306.09344*, 2023. 6, 2

[5] Rinon Gal, Yuval Alaluf, Yuval Atzmon, Or Patashnik, Amit H Bermano, Gal Chechik, and Daniel Cohen-Or. An image is worth one word: Personalizing text-to-image generation using textual inversion. *arXiv preprint arXiv:2208.01618*, 2022. 6, 1

[6] Jia Guo, Jiankang Deng, Alexandros Lattas, and Stefanos Zafeiriou. Sample and computation redistribution for efficient face detection. *arXiv preprint arXiv:2105.04714*, 2021. 3

[7] Hao He, Yinghao Xu, Yuwei Guo, Gordon Wetzstein, Bo Dai, Hongsheng Li, and Ceyuan Yang. Cameractrl: Enabling camera control for text-to-video generation. *arXiv preprint arXiv:2404.02101*, 2024. 1, 3

[8] Wenyi Hong, Wenmeng Yu, Xiaotao Gu, Guo Wang, Guobing Gan, Haomiao Tang, Jiale Cheng, Ji Qi, Junhui Ji, Li-hang Pan, et al. Glm-4.1 v-thinking: Towards versatile multimodal reasoning with scalable reinforcement learning. *arXiv preprint arXiv:2507.01006*, 2025. 6

[9] Jiancheng Huang, Mingfu Yan, Songyan Chen, Yi Huang, and Shifeng Chen. Magicfight: Personalized martial arts combat video generation. In *Proceedings of the 32nd ACM International Conference on Multimedia*, pages 10833–10842, 2024. 1

[10] Jiancheng Huang, Yi Huang, Jianzhuang Liu, Donghao Zhou, Yifan Liu, and Shifeng Chen. Dual-schedule inversion: Training-and tuning-free inversion for real image editing. In *2025 IEEE/CVF Winter Conference on Applications of Computer Vision (WACV)*, pages 660–669. IEEE, 2025. 2, 3

[11] Jiancheng Huang, Gengwei Zhang, Zequn Jie, Siyu Jiao, Yinlong Qian, Ling Chen, Yunchao Wei, and Lin Ma. M4v: Multi-modal mamba for text-to-video generation. *arXiv preprint arXiv:2506.10915*, 2025. 1

[12] Gottfried Jäger, Herbert W Franke, and Jean Stken. Generative photography: a systematic, constructive approach. *Leonardo*, 19(1):19–25, 1986. 1, 3

[13] Xuan Ju, Xian Liu, Xintao Wang, Yuxuan Bian, Ying Shan, and Qiang Xu. Brushnet: A plug-and-play image inpainting model with decomposed dual-branch diffusion. In *European Conference on Computer Vision*, pages 150–168. Springer, 2024. 1

[14] Christoph Klimmt, Christian Roth, Ivar Vermeulen, Peter Vorderer, and Franziska Susanne Roth. Forecasting the experience of future entertainment technology: “interactive storytelling” and media enjoyment. *Games and Culture*, 7(3):187–208, 2012. 1

[15] Weijie Kong, Qi Tian, Zijian Zhang, Rox Min, Zuozhuo Dai, Jin Zhou, Jiangfeng Xiong, Xin Li, Bo Wu, Jianwei Zhang, et al. Hunyuanyvideo: A systematic framework for large video generative models. *arXiv preprint arXiv:2412.03603*, 2024. 1

[16] Black Forest Labs, Stephen Batifol, Andreas Blattmann, Frederic Boesel, Saksham Consul, Cyril Diagne, Tim Dockhorn, Jack English, Zion English, Patrick Esser, et al. Flux. 1 kontext: Flow matching for in-context image generation and editing in latent space. *arXiv preprint arXiv:2506.15742*, 2025. 3, 6, 7, 8, 4

[17] Verica Lazova, Vladimir Guzov, Kyle Olszewski, Sergey Tulyakov, and Gerard Pons-Moll. Control-nerf: Editable feature volumes for scene rendering and manipulation. In *Proceedings of the IEEE/CVF Winter Conference on Applications of Computer Vision*, pages 4340–4350, 2023. 1, 3

[18] Wenbo Li, Zhe Lin, Kun Zhou, Lu Qi, Yi Wang, and Jiaya Jia. Mat: Mask-aware transformer for large hole image inpainting. In *Proceedings of the IEEE/CVF conference on computer vision and pattern recognition*, pages 10758–10768, 2022. 1

[19] Yitong Li, Zhe Gan, Yelong Shen, Jingjing Liu, Yu Cheng, Yuexin Wu, Lawrence Carin, David Carlson, and Jianfeng Gao. Storygan: A sequential conditional gan for story visualization. In *Proceedings of the IEEE/CVF conference on computer vision and pattern recognition*, pages 6329–6338, 2019. 1

[20] Zhen Li, Mingdeng Cao, Xintao Wang, Zhongang Qi, Ming-Ming Cheng, and Ying Shan. Photomaker: Customizing realistic human photos via stacked id embedding. In *Proceedings of the IEEE/CVF conference on computer vision and pattern recognition*, pages 8640–8650, 2024. 2

[21] Zongjian Li, Zheyuan Liu, Qihui Zhang, Bin Lin, Shanghai Yuan, Zhiyuan Yan, Yang Ye, Wangbo Yu, Yuwei Niu, and Li Yuan. Uniworld-v2: Reinforce image editing with diffusion negative-aware finetuning and mllm implicit feedback. *arXiv preprint arXiv:2510.16888*, 2025. 2, 3

[22] Lu Ling, Yichen Sheng, Zhi Tu, Wentian Zhao, Cheng Xin, Kun Wan, Lantao Yu, Qianyu Guo, Zixun Yu, Yawen Lu, et al. Dl3dv-10k: A large-scale scene dataset for deep learning-based 3d vision. In *Proceedings of the IEEE/CVF Conference on Computer Vision and Pattern Recognition*, pages 22160–22169, 2024. 2, 8

[23] Shilong Liu, Zhaoyang Zeng, Tianhe Ren, Feng Li, Hao Zhang, Jie Yang, Qing Jiang, Chunyuan Li, Jianwei Yang, Hang Su, et al. Grounding dino: Marrying dino with grounded pre-training for open-set object detection. In *European conference on computer vision*, pages 38–55. Springer, 2024. 3

[24] Jiawei Mao, Xiaoke Huang, Yunfei Xie, Yuanqi Chang, Mude Hui, Bingjie Xu, and Yuyin Zhou. Story-adapter: A training-free iterative framework for long story visualization. *arXiv preprint arXiv:2410.06244*, 2024. 1

[25] Xichen Pan, Pengda Qin, Yuhong Li, Hui Xue, and Wenhui Chen. Synthesizing coherent story with auto-regressive latent diffusion models. In *Proceedings of the IEEE/CVF Winter Conference on Applications of Computer Vision*, pages 2920–2930, 2024.

[26] Tanzila Rahman, Hsin-Ying Lee, Jian Ren, Sergey Tulyakov, Shweta Mahajan, and Leonid Sigal. Make-a-story: Visual memory conditioned consistent story generation. In *Proceedings of the IEEE/CVF conference on computer vision and pattern recognition*, pages 2493–2502, 2023. 1

[27] Nikhila Ravi, Valentin Gabeur, Yuan-Ting Hu, Ronghang Hu, Chaitanya Ryali, Tengyu Ma, Haitham Khedr, Roman Rädl, Chloe Rolland, Laura Gustafson, et al. Sam 2: Segment anything in images and videos. *arXiv preprint arXiv:2408.00714*, 2024. 3

[28] Jiangwei Ren, Xingyu Jiang, Zizhuo Li, Dingkang Liang, Xin Zhou, and Xiang Bai. Minima: Modality invariant image matching. In *Proceedings of the Computer Vision and Pattern Recognition Conference*, pages 23059–23068, 2025. 4, 6

[29] Team Seedream, Yunpeng Chen, Yu Gao, Lixue Gong, Meng Guo, Qiushan Guo, Zhiyao Guo, Xiaoxia Hou, Weilin Huang, Yixuan Huang, et al. Seedream 4.0: Toward next-generation multimodal image generation. *arXiv preprint arXiv:2509.20427*, 2025. 2, 3

[30] Quanjian Song, Mingbao Lin, Wengyi Zhan, Shuicheng Yan, Liujuan Cao, and Rongrong Ji. Univst: A unified framework for training-free localized video style transfer. *arXiv preprint arXiv:2410.20084*, 2024. 1

[31] Quanjian Song, Donghao Zhou, Jingyu Lin, Fei Shen, Jiaze Wang, Xiaowei Hu, Cunjian Chen, and Pheng-Ann Heng. Scenedecorator: Towards scene-oriented story generation with scene planning and scene consistency. *arXiv preprint arXiv:2510.22994*, 2025. 3, 6, 7, 2, 4

[32] Team Wan, Ang Wang, Baole Ai, Bin Wen, Chaojie Mao, Chen-Wei Xie, Di Chen, Feiwei Yu, Haiming Zhao, Jianxiao Yang, et al. Wan: Open and advanced large-scale video generative models. *arXiv preprint arXiv:2503.20314*, 2025. 1, 3, 4, 6

[33] Haiping Wang, Yuan Liu, Ziwei Liu, Wenping Wang, Zhen Dong, and Bisheng Yang. Vistadream: Sampling multiview consistent images for single-view scene reconstruction. In *Proceedings of the IEEE/CVF International Conference on Computer Vision*, pages 26772–26782, 2025. 3

[34] Qixun Wang, Xu Bai, Haofan Wang, Zekui Qin, Anthony Chen, Huaxia Li, Xu Tang, and Yao Hu. Instantid: Zero-shot identity-preserving generation in seconds. *arXiv preprint arXiv:2401.07519*, 2024. 2

[35] Zhouxia Wang, Xintao Wang, Liangbin Xie, Zhongang Qi, Ying Shan, Wenping Wang, and Ping Luo. Styleadapter: A unified stylized image generation model. *arXiv preprint arXiv:2309.01770*, 2023. 2

[36] Cong Wei, Zheyang Xiong, Weiming Ren, Xeron Du, Ge Zhang, and Wenhui Chen. Omnidit: Building image edit-ing generalist models through specialist supervision. In *The Thirteenth International Conference on Learning Representations*, 2024. 4, 5

[37] Chenfei Wu, Jiahao Li, Jingren Zhou, Junyang Lin, Kaiyuan Gao, Kun Yan, Sheng-ming Yin, Shuai Bai, Xiao Xu, Yilei Chen, et al. Qwen-image technical report. *arXiv preprint arXiv:2508.02324*, 2025. 3, 4, 6, 7

[38] Bin Xia, Bohao Peng, Yuechen Zhang, Junjia Huang, Jiyang Liu, Jingyao Li, Haoru Tan, Sitong Wu, Chengyao Wang, Yitong Wang, et al. Dreamomni2: Multimodal instruction-based editing and generation. *arXiv preprint arXiv:2510.06679*, 2025. 2, 3

[39] Guangxuan Xiao, Tianwei Yin, William T Freeman, Frédo Durand, and Song Han. Fastcomposer: Tuning-free multi-subject image generation with localized attention. *International Journal of Computer Vision*, 133(3):1175–1194, 2025. 2

[40] Shaoan Xie, Zhifei Zhang, Zhe Lin, Tobias Hinz, and Kun Zhang. Smartbrush: Text and shape guided object inpainting with diffusion model. In *Proceedings of the IEEE/CVF conference on computer vision and pattern recognition*, pages 22428–22437, 2023. 1

[41] Binxin Yang, Shuyang Gu, Bo Zhang, Ting Zhang, Xuejin Chen, Xiaoyan Sun, Dong Chen, and Fang Wen. Paint by example: Exemplar-based image editing with diffusion models. In *Proceedings of the IEEE/CVF conference on computer vision and pattern recognition*, pages 18381–18391, 2023. 1, 2

[42] Shuai Yang, Yuying Ge, Yang Li, Yukang Chen, Yixiao Ge, Ying Shan, and Ying-Cong Chen. Seed-story: Multimodal long story generation with large language model. In *Proceedings of the IEEE/CVF International Conference on Computer Vision*, pages 1850–1860, 2025. 1

[43] Yuanlin Yang, Quanjian Song, Zhexian Gao, Ge Wang, Shanshan Li, and Xiaoyan Zhang. Stydeco: Unsupervised style transfer with distilling priors and semantic decoupling. *arXiv preprint arXiv:2508.01215*, 2025. 2

[44] Zhuoyi Yang, Jiayan Teng, Wendi Zheng, Ming Ding, Shiyu Huang, Jiazheng Xu, Yuanming Yang, Wenyi Hong, Xiaohan Zhang, Guanyu Feng, et al. Cogvideox: Text-to-video diffusion models with an expert transformer. *arXiv preprint arXiv:2408.06072*, 2024. 1

[45] Hu Ye, Jun Zhang, Sibo Liu, Xiao Han, and Wei Yang. Ip-adapter: Text compatible image prompt adapter for text-to-image diffusion models. *arXiv preprint arXiv:2308.06721*, 2023. 2

[46] Lvmin Zhang, Anyi Rao, and Maneesh Agrawala. Adding conditional control to text-to-image diffusion models. In *Proceedings of the IEEE/CVF international conference on computer vision*, pages 3836–3847, 2023. 2

[47] Bolei Zhou, Agata Lapedriza, Aditya Khosla, Aude Oliva, and Antonio Torralba. Places: A 10 million image database for scene recognition. *IEEE Transactions on Pattern Analysis and Machine Intelligence*, 2017. 5

[48] Donghao Zhou, Jiancheng Huang, Jinbin Bai, Jiaze Wang, Hao Chen, Guangyong Chen, Xiaowei Hu, and Pheng-Ann Heng. Magictailor: Component-controllable person-

alization in text-to-image diffusion models. *arXiv preprint arXiv:2410.13370*, 2024. [2](#)

[49] Yupeng Zhou, Daquan Zhou, Ming-Ming Cheng, Jiashi Feng, and Qibin Hou. Storydiffusion: Consistent self-attention for long-range image and video generation. *Advances in Neural Information Processing Systems*, 37: 110315–110340, 2024. [1](#)

Geometry-Aware Scene-Consistent Image Generation

Supplementary Material

6. Evaluation Metric Selection

6.1. Text-Image Alignment Metric Selection

For evaluating text–image alignment, we compare two metrics: **CLIP-T** [5] and **Gemini 2.5 Flash Text–Image Alignment (G2.5F-TIA)** [3]. CLIP-T is a CLIP-based metric that computes global feature similarity between visual and textual inputs. Leveraging large-scale image–text pairs during training, CLIP-T excels at capturing coarse semantic correspondence between captions and images. However, in our experiments, we identified two notable limitations of CLIP-T in the context of fine-grained generative evaluation:

1. **Limited spatial relationship understanding.** CLIP-T is less sensitive to the relative positioning of objects or scene elements, which can lead to high similarity scores even when spatial arrangements deviate from the textual description.
2. **Limited action verification capability.** CLIP-T struggles to assess whether described actions or dynamic attributes in the text are correctly depicted in the image, often ignoring temporal or motion-related consistency.

To address these limitations, G2.5F-TIA employs a multi-modal reasoning approach that integrates spatial and action-aware alignment, yielding evaluations that better reflect fine-grained adherence to the textual prompt.

We present comparative cases, with two sets of generated results (Set A and Set B) shown in Fig. 5, where scores highlighted in bold indicate the set preferred by the respective metric (i.e., higher similarity depending on the convention). In the first two examples, the input text describes explicit spatial composition requirements for objects in the scene, with the spatial composition elements highlighted in red for clarity. Although the image in Set A violates the described spatial arrangement, CLIP-T still produces a high similarity score due to the presence of the correct object categories, whereas G2.5F-TIA assigns a lower score, accurately reflecting the mismatch in spatial configuration. In the latter two cases, the input text specifies an action attribute, with the action-related segments highlighted in red for clarity. The image in Set A fails to depict the described action, yet CLIP-T assigns a high score. G2.5F-TIA, however, correctly penalizes the violation, yielding scores that align more faithfully with human judgment and demonstrating greater sensitivity to fine-grained prompt adherence, particularly in scenarios involving spatial relationships and action verification.

To statistically validate these observations, we quantified the alignment of each metric with human preference. We compute the proportion of valid comparison pairs (pairs

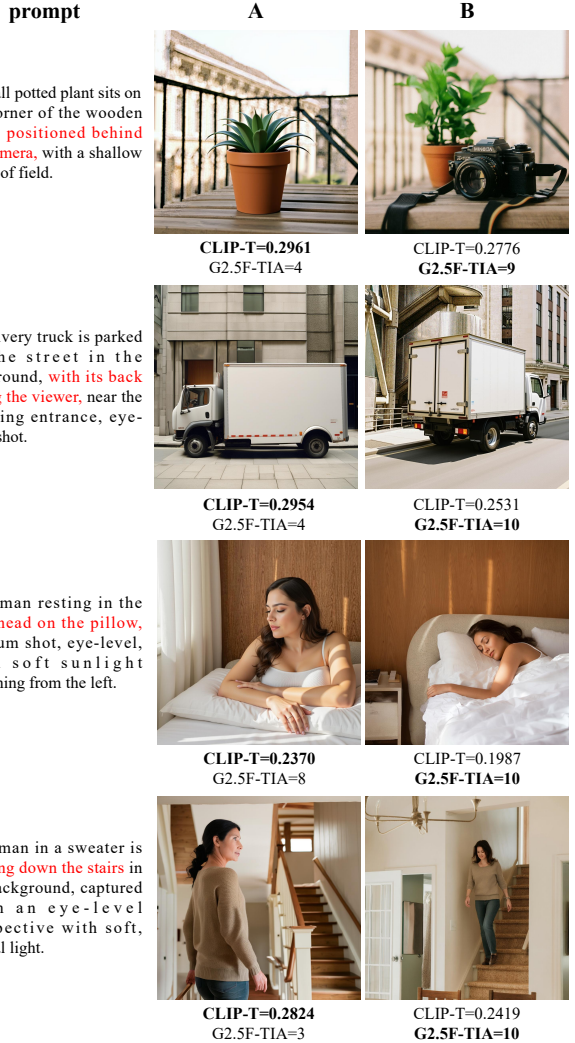


Figure 5. Comparison of text–image alignment evaluation metrics (CLIP-T [5]↑ vs. G2.5F-TIA [3]↑) on illustrative generation cases. Two experiment sets (A and B) are shown for each case; bold scores denote the set preferred by the respective metric. In the first two examples, spatial composition elements in the input text are highlighted in red, and in the latter two examples, action-related elements are highlighted in red. CLIP-T often fails to penalize violations of these spatial relationships or described actions, whereas G2.5F-TIA accounts for these fine-grained prompt attributes and yields scores that align more closely with human judgment.

with clear human preference) in which the best image selected by quantitative evaluation metric is the same as the best image selected by participants in the user study. As reported in Table 4, G2.5F-TIA achieves a pairwise

Table 4. Pairwise accuracy between quantitative evaluation metrics and user-study preferences for different tasks (higher is better).

Task	Metric	Pairwise Accuracy↑
Text-Image Alignment	G2.5F-TIA	83.36%
	CLIP-T	41.64%
Scene Alignment	G2.5F-SA	95.63%
	DreamSim	90.85%

accuracy of **83.36%**, significantly outperforming CLIP-T, which only reaches **41.64%**. This substantial gap confirms that CLIP-T often misaligns with human judgment on fine-grained details, whereas G2.5F-TIA serves as a robust proxy for human evaluation.

6.2. Scene Alignment Metric Selection

To evaluate scene alignment in our experiments, we considered several perceptual similarity metrics, including **DreamSim** [4] which is adopted in SceneDecorator [31] for measuring scene alignment and the multimodal large model **Gemini 2.5 Flash** [3]. DreamSim has shown strong performance on general image similarity benchmarks and has been used in prior work to assess scene-level coherence. However, in the context of our task, we observed a key limitation: sensitivity to permissible scene variations. While effective at capturing semantic and object-level similarity, DreamSim tends to produce disproportionately low scores when images differ due to permissible edits such as moderate viewpoint shifts, depth-of-field changes, or composition adjustments even if the underlying physical scene remains the same. This sensitivity reduces its reliability for evaluating scene alignment. In contrast, Gemini 2.5 Flash delivers more stable scores that align closely with human perceptual judgments in these scenarios. Given our task definition—allowing moderate viewpoint and composition changes while requiring global physical coherence—we confirm that the previously introduced Gemini 2.5 Flash Scene Alignment (G2.5F-SA) metric is the most reliable choice for evaluating scene alignment in this study.

Quantitative comparisons with DreamSim and G2.5F-SA are provided in Fig 6. We perform scene-consistent image generation from the reference image and produce two sets of results, denoted as Set A and Set B. For each set, the similarity scores computed by DreamSim and G2.5F-SA between the reference and the generated images are displayed below the corresponding samples. Scores that are highlighted in bold indicate the set preferred by the respective metric (higher similarity depending on the metric’s convention). Notably, DreamSim considers the images generated in Set B less similar to the reference, despite their visual closeness. As illustrated, common generative transfor-

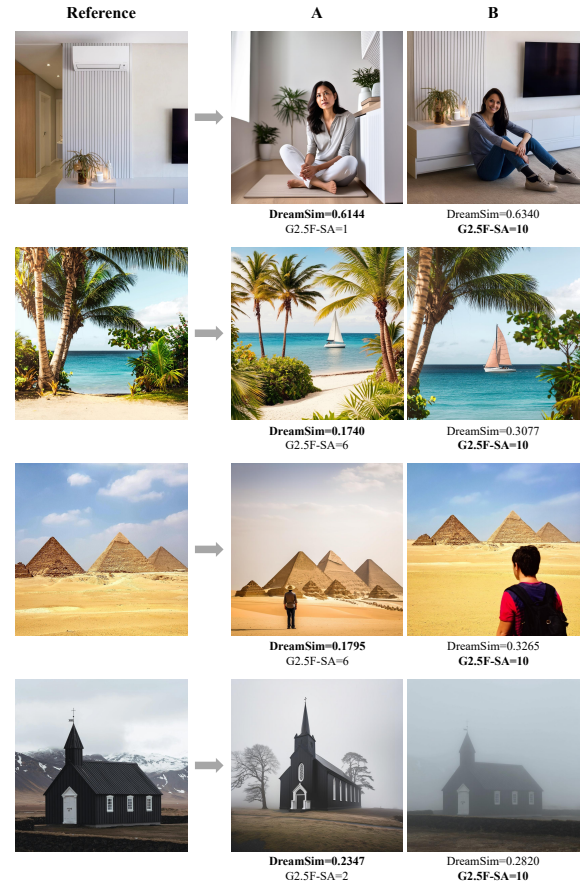


Figure 6. Comparison of scene-alignment metrics (DreamSim [4]↓ vs. G2.5F-SA [3]↑). Two experiment sets (A and B) are shown; in Set B, DreamSim reports higher distances despite the images being visually closer to the reference, whereas G2.5F-SA remains robust to scaling, viewpoint shifts, and defocus blur.

mations such as scaling, viewpoint shifts, or defocus blur can lead to such discrepancies in DreamSim’s evaluation. In contrast, G2.5F-SA explicitly accounts for these permissible variations, yielding evaluations that align more faithfully with human perceptual judgments.

We further corroborate this selection through quantitative correlation with user preferences, employing the same pairwise accuracy calculation protocol as described in the text-image alignment section. As summarized in Table 4, G2.5F-SA achieves a pairwise accuracy of **95.63%** with human judgments, surpassing DreamSim’s **90.85%**. While DreamSim is a strong baseline, the higher accuracy of G2.5F-SA indicates that its tolerance to permissible viewpoint and composition variations leads to evaluations that more faithfully reflect human perception of scene consistency. Thus, we adopt G2.5F-SA as our primary metric for evaluating scene alignment.

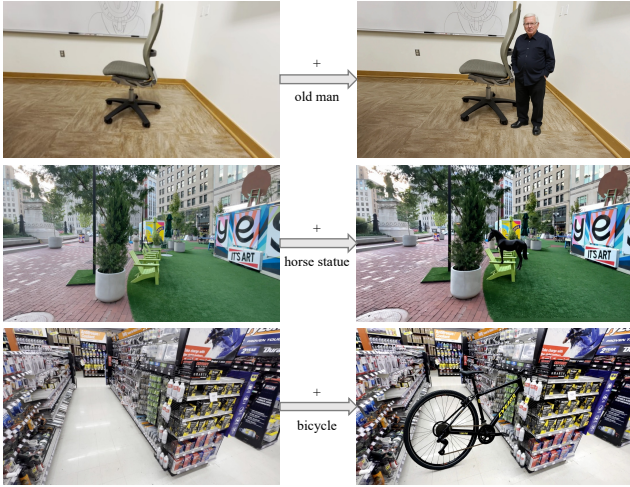


Figure 7. Examples of the DL3DV-10K-based data-construction baseline. For each example, the left image is the original DL3DV-10K scene image, and the right image is the composited result after inserting a new entity into the scene.

7. Visual Analysis of DL3DV-10K-based Composed Images

We visualize some examples of the DL3DV-10K-based data construction baseline in Figure 7, where entities (an old man, a horse statue, and a bicycle) are composited into real scenes. Across these cases, the inserted instances are frequently mis-scaled relative to nearby objects: in the first row, the person is rendered at approximately the same height as the adjacent chair, which is clearly implausible; in the second row, the horse statue is slightly under-scaled and fails to rest on the floor, instead seeming to hover around the chairs with incorrect spatial relationships; and in the third row, the bicycle is erroneously inserted so that its structure intersects the shelving unit. In addition, imperfect matting and lighting inconsistencies around object boundaries introduce visible halos and shading artifacts that break the photometric coherence of the scene. These instance-scale imbalances and compositing artifacts confirm that, although DL3DV-10K provides genuine multi-view coverage, the resulting images offer noisy supervision signals for geometry-aware scene-consistent image generation, consistent with the lower G2.5F-SA and G2.5F-TIA scores reported in Table 3 compared to our scene-consistent data construction pipeline.

8. Additional Qualitative Comparison Results

We provide additional qualitative comparisons with Qwen-Image-Edit [37], FLUX.1 Kontext Dev [16], and SceneDecorator [31] in Fig 8. These examples cover diverse text-guided editing scenarios and further highlight the limitations of the compared approaches, including unintended

background changes, reduced spatial accuracy, and appearance inconsistencies in scene elements. Our geometry-aware method consistently preserves fine-grained scene semantics and spatial alignment, producing outputs that remain faithful to the source scene while adhering closely to the editing prompts.

9. Details of Quantitative Evaluation

This section provides additional details on the automatic metrics and user study protocol used in Section 4.2. We explicitly describe the Gemini 2.5 Flash prompts used for automatic scoring and the annotation interface shown to human raters.

9.1. Details of Automatic Metrics

As described in Section 4.2, we utilize Gemini 2.5 Flash [3] as an evaluator to assess both scene alignment (G2.5F-SA) and text-image alignment (G2.5F-TIA). The exact prompts used to query the VLM are detailed in Table 5.

For scene alignment, the prompt explicitly instructs the model to tolerate intended edits such as object modifications and viewpoint changes, focusing the score on the preservation of the underlying physical scene. For text-image alignment, the prompt focuses solely on semantic adherence to the text instruction.

9.2. Details of User Study

To ensure a rigorous subjective evaluation, we conducted a user study involving 50 participants on an in-house crowdsourcing platform. The interface was designed to facilitate direct comparison between methods while maintaining a focus on the specific criteria defined in our task.

Interface Layout For each evaluation trial, the interface presented the reference image on the far left, with the target text instruction displayed at the top. To the right of the reference image, four candidate results generated by the compared methods were displayed in a horizontal row. The order of the candidate methods was randomized for every trial to prevent positional bias.

Annotation Instructions Participants were asked to evaluate the results based on a "Select All" mechanism. For each of the two criteria below, annotators were instructed to select all candidate images (Indices 1–4) that satisfied the requirement. The specific guidelines provided to the annotators were as follows:

1. Text Alignment:

Select all images from candidates 1–4 that are consistent with the textual description.

2. Scene Alignment:

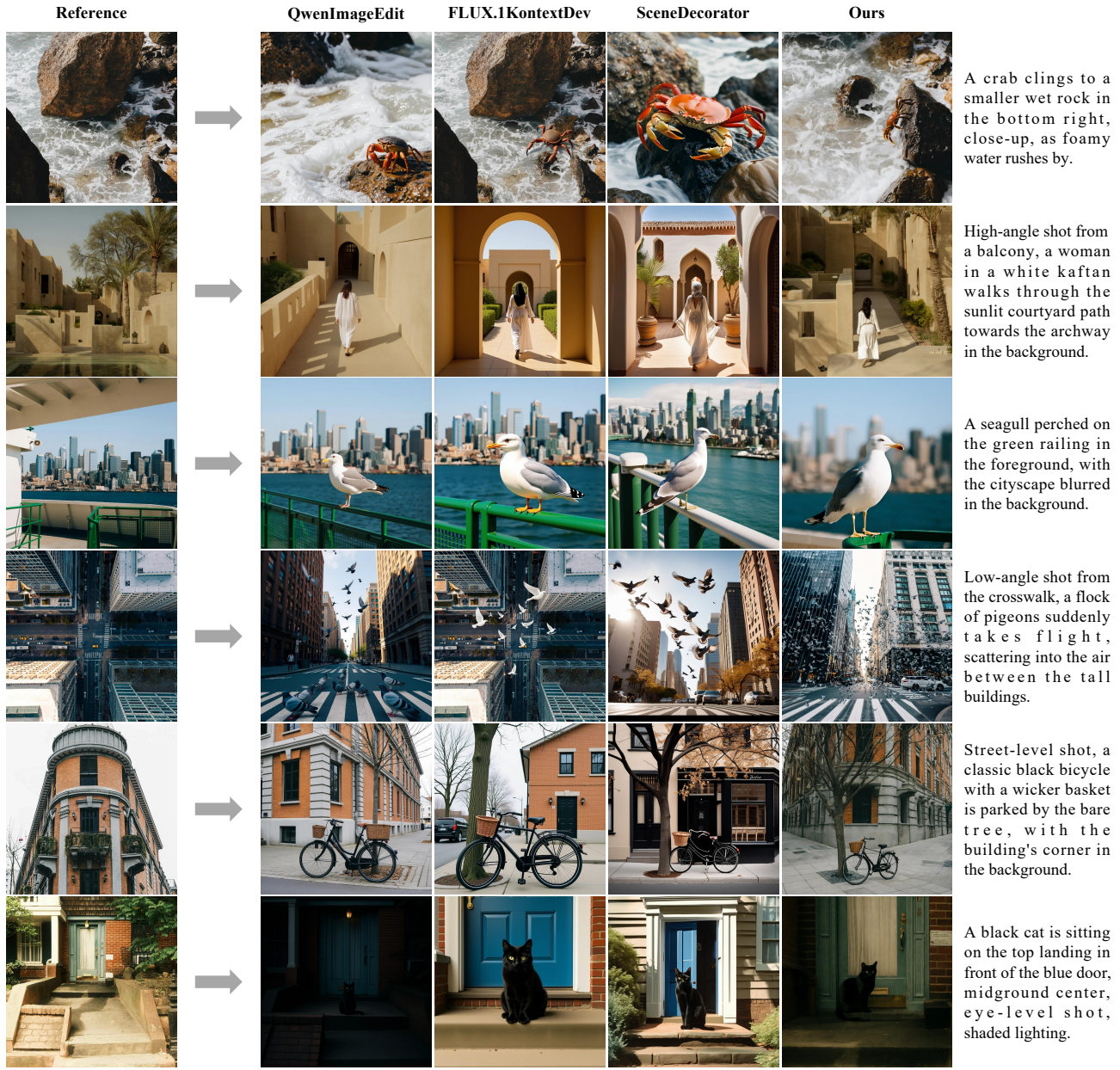


Figure 8. Additional qualitative comparisons of our method with Qwen-Image-Edit [37], FLUX.1 Kontext Dev [16], and SceneDecorator [31]. Our geometry-aware method better preserves spatial alignment and fine-grained scene semantics while avoiding unintended background changes.

Select all images from candidates 1–4 that remain consistent with the reference scene.

Guideline: Changes in viewpoint and composition are allowed. As long as the structure and details of the scene (e.g., positions of walls/furniture, decorative elements) remain unchanged, the image should be considered scene-consistent.

Data Aggregation Strategy To ensure evaluation reliability, each sample was assessed by three annotators, and we filtered the results to retain only methods with majority agreement. The final preference percentages in Table 1 were then derived using the temperature-scaled normalization scheme mentioned in the main paper. Specifically, for a prompt where k methods are retained after consensus filtering, we assign a score contribution $w = 1/k^\alpha$ (where

Metric	Input Prompt Template
G2.5F-SA (Scene Alignment)	<p>From scale 0 to 10: Give one score for how well the second image remains the same physical scene as the first image. Do not penalize normal edits: object additions/removals, close-up / background blur (DOF), zoom/rotation, and moderate viewpoint changes. (0 = completely different scene; 10 = clearly the same scene with only allowed edits.)</p> <p>Put the score in a list such that output score = [score].</p> <p>Text Prompt (use text only to understand intended edits): {prompt}</p>
G2.5F-TIA (Text-Image Alignment)	<p>From scale 0 to 10: A score from 0 to 10 will be given based on the success in following the prompt. (0 indicates that the image frames do not follow the prompt at all. 10 indicates the image frames follows the prompt perfectly.)</p> <p>Put the score in a list such that output score = [score].</p> <p>Text Prompt: {prompt}</p>

Table 5. **Prompts for Automatic Evaluation.** We employ Gemini 2.5 Flash to evaluate scene alignment and text-image alignment. The placeholders {prompt} are replaced with the specific textual instruction for each test case.

$\alpha = 0.8$ serves as the temperature factor) to balance between approval and fractional voting, followed by normalization.

10. Supplementary Videos

To further demonstrate the effectiveness of our geometry-aware framework in maintaining scene consistency across diverse viewpoints, and to illustrate its application in synthesizing start and end frames for image-to-video generation, we provide two videos in the accompanying supplementary folder. These videos were synthesized using the Kling image-to-video model, utilizing keyframes produced by our method. In the first sequence, the start frame is generated by our method while the final frame is the original scene. Conversely, the second sequence begins with the original scene, with the intermediate and final frames being generated views. Across both videos, the interpolated trajectories—including long-range camera motions such as zoom-outs and large viewpoint changes—remain stable. Crucially, the background geometry is preserved without noticeable texture flickering or structural drift, highlighting the suitability of our method as a robust keyframe generator for long-duration video editing.